Ecogenomics and potential biogeochemical impacts of globally abundant ocean viruses

Simon Roux[1], Jennifer R. Brum[1], Bas E. Dutilh[2,3,4], Shinichi Sunagawa[5,‡], Melissa B. Duhaime[6], Alexander Loy[7,8], Bonnie T. Poulos[9], Natalie Solonenko[1], Elena Lara[10,11], Julie Poulain[12], Stéphane Pesant[13,14], Stefanie Kandels-Lewis[5,15], Céline Dimier[16,17], Marc Picheral[18,19], Sarah Searson[18,19,20], Corinne Cruaud[12], Adriana Alberti[12], Carlos M. Duarte[21,22], Josep M. Gasol[10], Dolors Vaqué[10], *Tara* Oceans Coordinators[†], Peer Bork[5,23], Silvia G. Acinas[10], Patrick Wincker[12,24,25], Matthew B. Sullivan[1,26*]

[1] Department of Microbiology, The Ohio State University, Columbus, OH, USA
[2] Theoretical Biology and Bioinformatics, Utrecht University, Utrecht, The Netherlands
[3] Centre for Molecular and Biomolecular Informatics, Radboud University Medical Centre, Nijmegen, The Netherlands
[4] Department of Marine Biology, Federal University of Rio de Janeiro, Rio de Janeiro, Brazil
[5] Structural and Computational Biology, European Molecular Biology Laboratory, Heidelberg, Germany
[6] Department of Ecology and Evolutionary Biology, University of Michigan, MI, USA
[7] Division of Microbial Ecology, Department of Microbiology and Ecosystem Science, Research Network Chemistry Meets Microbiology, University of Vienna, Vienna, Austria
[8] Austrian Polar Research Institute, Vienna, Austria
[9] Department of Ecology and Evolutionary Biology, University of Arizona, Tucson, AZ, USA
[10] Department of Marine Biology and Oceanography, Institut de Ciències del Mar (CSIC), Barcelona, Spain
[11] Institute of Marine Sciences (CNR-ISMAR), National Research Council, Venezia, Italy
[12] CEA - Institut de Génomique, GENOSCOPE, Evry, France
[13] PANGAEA, Data Publisher for Earth and Environmental Science, University of Bremen, Bremen, Germany
[33] MARUM, Bremen University, Bremen, Germany
[15] Directors' Research European Molecular Biology Laboratory, Heidelberg, Germany
[16] CNRS, UMR 7144, EPEP, Station Biologique de Roscoff, Roscoff, France
[17] Sorbonne Universités, UPMC Univ Paris 06, UMR 7144, Station Biologique de Roscoff, Roscoff, France
[18] CNRS, UMR 7093, Laboratoire d'océanographie de Villefranche (LOV), Observatoire Océanologique, Villefranche-sur-mer, France
[19] Sorbonne Universités, UPMC Univ Paris 06, UMR 7093, Observatoire Océanologique, Villefranche-sur-mer, France.
[20] Department of Oceanography, University of Hawaii, Honolulu, Hawaii, USA
[21] Mediterranean Institute of Advanced Studies, CSIC-UiB, Esporles, Mallorca, Spain
[22] King Abdullah University of Science and Technology (KAUST), Red Sea Research Center (RSRC), Thuwal, Saudi Arabia
[23] Max-Delbrück-Centre for Molecular Medicine, 13092 Berlin, Germany
[24] CNRS, UMR 8030, CP5706, Evry, France
[25] Université d'Evry, UMR 8030, CP5706, Evry, France
[26] Department of Civil, Environmental and Geodetic Engineering, The Ohio State University, Columbus, OH, USA

[†]*Tara* Oceans coordinators and affiliations are listed in the Supplementary Information.

‡ Current address: Institute of Microbiology, ETH Zurich, Zurich, Switzerland

[*] correspondence to mbsulli@gmail.com

Abstract

Ocean microbes drive global-scale biogeochemical cycling[1], but do so under constraints imposed by viruses on community composition, metabolic activity, and evolutionary trajectories[2,3]. Due to sampling and cultivation challenges, genome-level viral diversity remains poorly described and grossly understudied in nature such that <1% of observed surface ocean viruses are 'known'[4]. Here we assemble complete genomes and large genomic fragments from both surface and deep ocean viruses sampled during the *Tara* Oceans and *Malaspina* research expeditions[5,6] and analyze the resulting Global Ocean Viromes (GOV) dataset to present a global map of abundant, double stranded DNA (dsDNA) viruses complete with genomic and ecological contexts. A total of 15,222 epi- and mesopelagic viral populations were identified that comprised 867 viral clusters (VCs, approximately genus-level groups[7,8]). This roughly triples the number of ocean viral populations[4], doubles candidate bacterial and archaeal virus genera[8], and near-completely samples epipelagic communities at both the population and VC level. Thirty-eight of the 867 VCs were locally or globally abundant and together accounted for nearly half of the viral populations in any GOV sample. While two thirds of them represent newly described viruses that lacked any cultivated representative, most could be computationally linked to dominant, ecologically relevant microbial hosts. Moreover, we identified 243 viral-encoded auxiliary metabolic genes (AMGs), only 95 of which were known. Deeper analyses of four of these AMGs (*dsr*C, *sox*YZ, P-II and *amo*C) revealed that abundant viruses may directly manipulate sulfur and nitrogen cycling throughout the epipelagic ocean. This viral catalog and functional analyses provide a critically-needed foundation to begin meaningfully integrating viruses into ecosystem models as key players in nutrient cycling and trophic networks.

Main text

A fundamental bottleneck preventing the incorporation of viruses of microbes into ecosystem models is the lack of host-contextualized quantitative surveys of viral diversity in nature. This is because (i) most naturally-occurring microbes and viruses are not currently cultivated, and (ii) viruses lack a universally conserved marker gene, which precludes PCR-based surveys of uncultivated diversity[3]. While viral metagenomics (viromics) was introduced to circumvent these issues, early datasets were fragmented and only suitable for descriptive gene-level analyses that were prohibitively database-biased[3]. Subsequent experimental, technological, and analytical improvements enabled viral population ecology through the availability of genomic information[3,9–11]. For example, 1,148 large viral genome fragments captured in a fosmid library from Mediterranean Sea microbes revealed remarkable viral diversity, with some genomes appearing globally distributed based upon analysis of six available viral metagenomes[9]. Similarly, 69 viral reference genomes assembled from single-cell samples helped elucidate the ecology, evolution and potential biogeochemical impacts of uncultivated viruses infecting an uncultivated anaerobic chemoautotroph[11]. Finally, metagenomic approaches are now quantitative, at least for dsDNA templates[3], and themselves provide genomic information on uncultivated viruses. For example, 42 surface ocean viral metagenomes in the *Tara* Oceans Viromes (TOV) dataset revealed the global underlying structure of these communities, and identified 5,476 viral populations, only 39 of which were previously known[4].

Here we further identify ocean viral populations, determine and characterize the most abundant and widespread dsDNA ocean viral types, and analyze viral-encoded AMGs and their distributions to propose new means by which viruses likely modulate microbial biogeochemistry. We do so by analyzing the Global Oceans Viromes (GOV) dataset, which augments TOV with 61 samples to better represent the surface and deep oceans, and now totals 104 viromes and 925 Gbp of sequencing data (Supplementary Table 1). Further, upgraded analytical approaches including cross-assembly[12] and genome binning[13] improved genomic representation of sampled viruses (see Supplementary Text for details on the dataset generation process). From 1,380,834 contigs which recruited 67% of the reads, we identified 15,280 viral populations (Fig. 1A, see Supplementary Fig. 1 for viral population

definition explanation). This expands ocean viral populations nearly 3-fold over the prior TOV dataset[4], while also improving average contig lengths and genomic context 2.5-fold for TOV-known populations (Supplementary Table 2). Rarefaction analyses show that while mesopelagic viral communities remain undersampled, epipelagic viral communities now appear near-completely sampled (Extended Data Fig. 1A). Because bathypelagic communities were underrepresented due to cellular contamination, we focused the remaining analyses on 15,222 non-bathypelagic viral populations.

We first categorized viral populations into viral clusters, or VCs using shared gene content information and network analytics[7] (see Supplementary Fig. 1 for VC definition schematic). This method starts from genome fragments (≥10kb) and results in VCs approximately equivalent to known viral genera[7,8]. Clustering of the 15,222 GOV viral populations with 15,929 publicly available bacterial and archaeal viruses revealed 1,259 VCs (see Supplementary Table 3, Supplementary Text & Extended Data Fig. 2 for comparison with alternative classification methods). Of these, 658 included exclusively GOV sequences, which approximately doubles known bacterial and archaeal virus genera[8], and another 209 VCs contained at least one GOV sequence (Fig. 1B). As with viral populations, rarefaction analyses suggested that VC diversity was undersampled in mesopelagic waters, but near-completely sampled in epipelagic waters (Extended Data Fig. 1B).

We next identified the most abundant and widespread VCs based on read recruitment of VC members. In each sample, a fraction of the VCs were identified as abundant based on their cumulative contribution to sample diversity (estimated with Simpson Index, abundant VCs represent 80% of the total sample diversity, Extended Data Fig. 1C). By these criteria, only 38 of 867 observed VCs were abundant in two or more stations, and together recruited an average of 50% and 35% of reads from viral populations for epipelagic and mesopelagic samples, respectively (Supplementary Table 3). Four of these 38 abundant VCs were also relatively ubiquitous as they were abundant in more than 25 stations, and 62 of the 91 non-bathypelagic samples were dominated by 1 of these 4 VCs (Fig. 2 A & B). Among the 38 abundant VCs, only 2 corresponded to well-studied viruses, from the T4 superfamily[14,15] (VC_2, 1 of the 4 ubiquitous) and the *T7virus* genus[16] (VC_9). Eight represented known but unclassified viral isolates, 10 included viruses known only from environmental sequencing[9,10], and the remaining 18 VCs were completely novel (Fig. 2C, Extended Data Fig. 3).

Given this global map of the dominant dsDNA viral types in the oceans, we next sought to identify the range of hosts these viruses infect. This is challenging, as culture-based methods insufficiently capture naturally-occurring diversity, whereas metagenomic approaches broadly survey viral diversity but often without host information. Fortunately, sequence-based approaches are emerging that examine similarities between (i) viral genomes and host CRISPR spacers[17], (ii) viral and microbial genomes due to integrated prophages or gene transfers[9], and (iii) viral and host genome nucleotide signatures (here, tetranucleotide frequencies[8], see Supplementary Table 4 and Supplementary Text for discussion of the accuracy/sensitivity of *in silico* host prediction methods). We applied all 3 methods to GOV to predict hosts at the phylum level, or class level for Proteobacteria (Supplementary Table 5), then summarized these results at the VC level. This led to host range predictions for 392 of 867 VCs – all with confidence assessed by comparison to a null model (Supplementary Fig. 2 and Supplementary Table 3).

The hosts of the 38 globally abundant VCs were largely restricted to abundant and widespread epipelagic-ocean microbes that were previously identified via $_{mi}$Tag-based OTU counts in *Tara* Oceans microbial metagenomes[18]. Notably, the 4 ubiquitous and abundant VCs were predicted to infect 7 of the 8 globally abundant microbial groups (Actinobacteria, Alpha-, Delta-, and Gammaproteobacteria, Bacteroidetes, Cyanobacteria, Deferribacteres; Fig. 2C, Extended Data Fig. 4). The 8th abundant microbial group, Euryarchaeota, was not linked to these 4 VCs, but was predicted as a host for 3 of the 34 other abundant VCs (VC_3, VC_27, and VC_63, Extended Data Fig. 3). Among the 38 abundant VCs, the number of VCs predicted to infect a given microbial host phylum (or class for Proteobacteria) was positively correlated with host global richness rather than relative abundance (Extended Data Fig. 4B). This suggests that, likely because ocean viruses appear globally distributed[4], widespread and

abundant hosts that are minimally diverse (e.g. Cyanobacteria) provide few viral niches, whereas more diverse host groups, even at lower abundance (e.g. Betaproteobacteria), provide more opportunity for viral niche differentiation. Hence, these host associations provide critically-needed empirical support for hypotheses derived from global virus-host network models[19].

Having mapped viral diversity and predicted virus-host pairings, we next sought to identify virus-encoded AMGs that might modify host metabolism during infection and likely impact biogeochemistry. To maximize AMG detection, all 298,383 viral contigs >1.5kb were examined, including small contigs not associated with a viral population. This revealed 243 putative AMGs (Supplementary Table 6). While 95 of these AMGs were known (reviewed in ref. [20]), others offer insights into how viruses may directly manipulate microbial metabolisms. Here we focus on 4 (*dsr*C, *sox*YZ, P-II and *amo*C; see Extended Data Table 1, Supplementary Figs. 3-6 and Supplementary Text for functional affiliation of these AMGs) because of their putative roles in sulfur or nitrogen cycling. Three of these are not known in viruses, and one, *dsrC*, has only been observed in viruses from anoxic deep-sea environments[11,21].

Sulfur oxidation in seawater involves two central microbial pathways – dissimilatory sulfur reductase (Dsr) and sulfur oxidation (Sox)[22] – and GOV AMG analyses revealed that epipelagic viruses encode key genes for each. First, 11 *dsrC*-like genes were identified in viral contigs (Extended Data Fig. 5). The Dsr operon is used by sulfate/sulfite-reducing microbes in anoxic environments, as well as sulfur-oxidizing bacteria in oxic and anoxic environments (Fig. 3A)[22]. DsrC, specifically, provides sulfur to DsrAB-sulfite reductase for processing through a conserved C-terminal motif ($Cys_BX_{10}Cys_A$), and dictates sulfur metabolism rates[23]. Other DsrC-like proteins (also known as TusE) lack Cys_B and instead participate to tRNA modification[24]. In GOV, four clades of DsrC-like sequences were similar to TusE (DsrC-1 to DsrC-4), whereas the fifth (DsrC-5) was similar to *bona fide* DsrC (Extended Data Fig. 5, Extended Data Table 1, Supplementary Fig. 3, and Supplementary text). Second, 4 *soxYZ* genes were identified on viral contigs (Extended Data Fig. 6). Like DsrC, SoxYZ is an important sulfur carrier harboring a conserved functional motif identified in all GOV SoxYZ proteins (Fig. 3A, Supplementary Fig. 4, and Supplementary text)[25].

Other AMGs suggest marine viruses may manipulate nitrogen cycling. First, 10 GOV contigs encoded P-II, a gene widespread across bacteria and archaea and central in nitrogen metabolism regulation (Fig. 3B)[26]. Three AMG clades (P-II-1, P-II-2, and P-II-4) displayed both P-II conserved motifs and had predicted structures similar to bona fide P-II, whereas the fourth clade (P-II-3) is functionally ambiguous as it lacked a conserved motif (Supplementary Fig. 5, and Supplementary text). Second, two P-II AMG clades (P-II-1 and P-II-4) were proximal to an ammonium transporter gene, *amt*, in GOV contigs (Extended Data Fig. 7). In bacteria, such an arrangement is a signature of P-II-like genes that specifically activate alternative nitrogen production and ammonia uptake pathways during nitrogen starvation[26]. Third, one GOV contig included *amo*C, encoding the subunit C of ammonia monooxygenase, suggesting a role in ammonia oxidation[27]. While functional annotation is challenging for these genes[27], and functional motifs are not yet known, the translated AMG was 94% identical to functional AmoC from Thaumarchaeota – a level of identity only observed among expressed and functional AMGs (Extended Data Fig. 8, Supplementary Fig. 6, and Supplementary text).

Next, we investigated the origin, evolutionary history, and diversity of these AMGs in epipelagic viruses (see Supplementary Text for additional discussion about taxonomic affiliation and host prediction for AMG-containing GOV sequences). The 15 GOV contigs encoding *dsrC* or *soxYZ* genes, when affiliated, were all associated with members of the abundant and ubiquitous VC_2 (T4 superfamily, Extended Data Fig. 5 and 6, Extended Data Table 1). Phylogenies suggested that these viruses obtained AMGs from S-oxidizing proteobacterial hosts, with likely a single transfer event for *sox*YZ and two for *dsr*C (Extended Data Fig. 5 and 6). Among the latter, the bona fide S-oxidation DsrC-5 was most closely related to a clade of uncultivated S-oxidizing Gammaproteobacteria (MED13k09, Supplementary Fig. 7). These bacteria are widespread in the epipelagic ocean[28] and suspected to degrade dimethyl sulfide, a key reduced sulfur species involved in ocean-to-atmosphere

sulfur transport and cloud formation. If confirmed, DsrC5-encoding viruses infecting these bacteria would impact critical sulfur cycling steps throughout surface waters. In contrast to sulfur AMGs, phylogenies suggest that P-II AMGs originated from diverse viruses (6 VCs including the abundant VC_2 and VC_12), and were acquired at least 4 times independently from Bacteroidetes, Proteobacteria, and possibly Verrucomicrobia (Extended Data Fig. 7, and Supplementary Text). Finally, while a single *amoC* AMG offers only preliminary evaluation of its evolutionary history, this *amo*C-encoding contig appears to represent novel and rare archaeal dsDNA viruses (VC_623), predicted to infect ammonia-oxidizing Thaumarchaeota, known for their major role in global nitrification[29] (Extended Data Fig. 8).

Finally, we investigated the ecology of viruses encoding these AMGs by mapping their distribution across GOV. Seven AMG clades were geographically restricted (DsrC-unc, DsrC-1, DsrC-2, DsrC-4, P-II-2, P-II-3, and *amo*C), and 5 were widespread throughout epipelagic (DsrC-3, DsrC-5, SoxYZ, P-II-1) or mesopelagic (P-II-4) waters (Fig. 3C). All widespread epipelagic AMGs were detected in waters of mid-range temperatures. In contrast, DsrC-5 and SoxYZ were predominantly detected in low-nutrient conditions, while P-II-1 was predominantly detected in high-nutrient conditions (Fig. 3D, Extended Data Fig. 9). Thus, we hypothesize that viruses utilize DsrC-5 or SoxYZ to boost sulfur oxidation rates when infecting sulfur oxidizers in low-nutrient conditions, and P-II under high-nutrient conditions. The latter could be useful to viruses by activating expensive alternative N-producing pathways typically used only under N-starvation conditions[26]. Consistent with this, metatranscriptomes from three low-nutrient stations (11_SRF in Mediterranean Sea, 39_DCM in Arabian Sea, and 151_SRF in Atlantic Ocean) revealed expression of viral homologs of *dsr*C and *sox*YZ but not of P-II (Extended Data Table 1).

Overall, this systematically collected and processed GOV dataset provides a critical resource for marine microbiology. This map of global dsDNA ocean viral diversity, at both the population and VC level, and viral-encoded AMGs brings global ecological context to abundant surface and deep ocean viruses. Both will also help interpret future (meta)genomic datasets and select experimental systems to develop. Together with recent experimental, informatic and theoretical advances[3,12,30], this fundamental resource will accelerate the field towards understanding and dynamically predicting the roles and planetary impacts of viruses in nature.

Methods

Sample collection and processing

Tara *Oceans expedition*

Ninety samples were collected between October 10, 2009, and December 12, 2011, at 45 locations throughout the world's oceans (Supplementary Table 1) through the *Tara* Oceans Expedition[32]. These included samples from a range of depths: surface, deep chlorophyll maximum, bottom of mixed layer when no deep chlorophyll maximum was observed (Station 123, 124, and 125), and mesopelagic samples. The sampling stations were located in 7 oceans and seas, 4 different biomes and 14 Longhurst oceanographic provinces (Supplementary Table 1). For TARA station 100, two different peaks of chlorophyll were observed, so two samples were taken at the shallow (100_DCM) and deep (100_dDCM) chlorophyll maximum. For each sample, 20 L of seawater were 0.22 µm-filtered and viruses were concentrated from the filtrate using iron chloride flocculation[33] followed by storage at 4ºC. After resuspension in ascorbic-EDTA buffer (0.1 M EDTA, 0.2 M Mg, 0.2 M ascorbic acid, pH 6.0), viral particles were concentrated using Amicon Ultra 100 kDa centrifugal devices (Millipore), treated with DNase I (100U/mL) followed by the addition of 0.1M EDTA and 0.1M EGTA to halt enzyme activity, and extracted as previously described[34]. Briefly, viral particle suspensions were treated with Wizard PCR Preps DNA Purification Resin (Promega, WI, USA) at a ratio of 0.5 mL sample to 1 mL resin, and eluted with TE buffer (10 mM Tris, pH 7.5, 1 mM EDTA) using Wizard Minicolumns. Extracted DNA was Covaris-sheared and size selected to 160–180 bp, followed by amplification and ligation per the standard Illumina protocol. Sequencing was done on a HiSeq 2000 system (101 bp, paired end reads) at the Genoscope facilities (Paris, France).

Temperature, salinity, and oxygen data were collected from each station using a CTD (Sea-Bird Electronics, Bellevue, WA, USA; SBE 911plus with Searam recorder) and dissolved oxygen sensor (Sea-Bird Electronics; SBE 43). Nutrient concentrations were determined using segmented flow analysis[35] and included nitrite, phosphate, nitrite plus nitrate, and silica. Nutrient concentrations below the detection limit (0.02 µmol kg^{-1}) are reported as 0.02 µmol kg^{-1}. All data from the Tara Oceans expedition are available from ENA (for nucleotide) and from PANGAEA (for environmental, biogeochemical, taxonomic and morphological data)[36–38].

Malaspina expedition

Thirteen bathypelagic samples and one mesopelagic sample were collected between April 19, 2011 and July 11, 2011 during the Malaspina 2010 global circumnavigation covering the Pacific and the North Atlantic Ocean. All samples were taken at 4,000 m depth except two samples from stations 81 and 82 collected at 3,500 and 2,150 m respectively (Supplementary Table 1). Additionally, Station M114 was sampled at the OMZ region at 294 m depth. For each sample, 80 L of seawater were 0.22 µm-filtered and viruses were concentrated from the filtrate using iron chloride flocculation[33] followed by storage at 4°C. More details about the sampling and additional variables used in the Malaspina expedition can be found in ref. [39]. Further processing was done as for the *Tara* Oceans samples, except that Illumina sequencing was done at DOE JGI Institute (151 bp, paired end reads).

Dataset generation

Contigs assembly

An overview of the contigs generation process is provided in Supplementary Fig. 8. The first step consisted in the generation of a set of contigs using as many reads as possible from the 104 oceanic viromes, including 74 epipelagic and 16 mesopelagic samples from the *Tara* Oceans expedition[5], and 1 mesopelagic and 13 bathypelagic from the Malaspina expedition[6]. This set of contigs was generated through an iterative cross-assembly[12] (using MOCAT[40] and Idba_ud[41], Supplementary Fig. 8) as follows: (i) high-quality (HQ) reads were first assembled sample by sample with the MOCAT pipeline

as described in[18], (ii) all reads not mapping (Bowtie 2[42], options --sensitive, -X 2000, and --non-deterministic, other parameters at default) to a MOCAT contig (by which we denote 'scaftigs', that is, contigs that were extended and linked using the paired-end information of sequencing read[43]) were assembled sample by sample with Idba_ud (iterative k-mer assembly, with k-mer increasing from 20 to 100 by step of 20), (iii) all reads remaining unmapped to any contig were then pooled by Longhurst province (i.e. unmapped reads from samples corresponding to the same Longhurst province were gathered) and assembled with Idba_ud (with the same parameters as above), and (iv) all remaining reads unmapped from every samples were gathered for a final cross-assembly (using Idba_ud). This resulted in 10,845,515 contigs (Supplementary Fig. 8B).

Genome binning and re-assembly

The contigs assembled from the marine viral metagenomes might still contain redundant sequences derived from the same, or closely related populations. We set out to merge contigs derived from the same population into clusters representing population genomes. To this end, contig sequences were first clustered at 95% global average nucleotide identity (ANI) with cd-hit-est[44](options -c 0.95 -G 1 -n 10 -mask NX, Supplementary Fig. 8B), resulting in 10,578,271 non-redundant genome fragments. Next, we used co-abundance (i.e. correlation between abundance profiles estimated by reads mapping) and nucleotide usage profiles of the non-redundant contigs to further identify contigs derived from the same populations with Metabat[45]. Briefly, Metabat uses Pearson correlation between coverage profiles (determined from the mapping of HQ reads of each sample to the contigs with Bowtie 2[42], options --sensitive, -X 2000, and --non-deterministic, other parameters at default) and tetranucleotide frequencies to identify contigs originating from the same genome (Metabat parameters: 98% minimum correlation, mode "sensitive", see Supplementary Text for more detail about the selection of these parameters). The 8,744 bins generated, including 3,376,683 contigs, were further analyzed, alongside 623,665 contigs not included in any genome bin but ≥1.5kb.

In an attempt to better assemble these genome bins, two additional sets of contigs were generated for each genome bin (beyond the set of initial contigs binned by Metabat[45]), based on the de novo assembly of (i) all reads mapping to the contigs in the genome bin, and (ii) only reads from the sample displaying the highest coverage for the genome bin (both assemblies with Idba_ud[41], Supplementary Fig. 8C). The latter might be expected to lead to the "cleanest" genome assembly because it includes the minimum between-sample sequence variation, lowering the probability of generating chimeric contig[46]. The former may be necessary if the virus is locally rare, so that sequences from multiple metagenomes are needed to achieve complete genome coverage. Thus, if the assembly from the single "highest coverage sample" was improved or equivalent to the initial assembly (longest contig in the new assembly representing ≥95% of the longest contig in the initial assembly), this set of contigs was selected as the sequence for this bin (n=6,423). This optimal single-sample assembly was thus privileged compared to a cross-assembly (either based on the initial contigs or on the re-assembly of all sequences aligned to that bin). Otherwise, the "all samples" bin re-assembly was selected if equivalent or better than the initial assembly (longest contig representing ≥95% of the longest initial contig, n=999). The assumption that cross-assembly would be needed for locally rare viruses, without a high-coverage sample, was confirmed by the comparison between the highest coverage of these two types of bins: on average, bins for which the "optimal" assembly were selected displayed a maximum coverage of 5.47 per Gb of metagenome, while the bins for which the "cross-assembly" was selected displayed a maximum coverage of 1.37 per Gb of metagenome (Supplementary Table 2). Finally, if both re-assemblies yielded a longest contig smaller (<95%) than the one in the initial assembly, the bin was considered as a false positive (i.e. binning of contigs from multiple genomes, n=1,356), and contigs from the initial assembly were considered as "unbinned" (263,006 contigs, added to the 623,665 contigs ≥1.5kb initially retained as "unbinned").

Identification of viral contigs and delineation of viral populations

Despite efforts to completely remove cellular DNA during sample preparation, the resulting viral metagenomic datasets will only ever be enriched for viruses[47]. Thus, assembled sequences in the GOV dataset were *in silico* filtered *a posteriori* to identify and remove clearly non-viral signal. In this way, our purification methods should have greatly enriched for viruses, but the *in silico* decontamination step served as a back-up for problematic samples. Together these two "filters" mean that virtually no known cellular signal should have been considered in our analyses. For the *in silico* cleaning step, VirSorter[48] was used to identify and remove microbial contigs using the "virome decontamination" mode, with every contig ≥10kb and not identified as a viral contig being considered as a microbial contig. Sequences with a prophage predicted were manually curated to distinguish actual prophages (i.e. viral regions within a microbial contig) from contigs that belonged to a viral genome and were wrongly predicted as a prophage. Contigs originating from an eukaryotic virus were identified based on best BLAST hit affiliation of the contig predicted genes against NCBI RefseqVirus (see Supplementary Text).

The genome bins were affiliated as microbial (if 1 or more contigs were identified as microbial, n=1,763), eukaryotic virus (if contigs affiliated as eukaryotic virus comprised more than 10kb or more than 25% of the genome bin total length, n=962) or viral (i.e. archaeal and bacterial viruses, n=4,341), with the 356 remaining bins, lacking a contig long enough for an accurate affiliation, considered as "unknown" (see Supplementary Text).

Viral bins were then refined to evaluate if they corresponded to a single or a mix of viral population(s). To that end, the Pearson correlation and Euclidean distance between abundance profiles (i.e. profile of the contig average coverage depth across the 104 samples) of bin members and the bin seed (i.e. the largest contig) were computed, and a single-copy viral marker gene (TerL) was identified in binned contigs (Supplementary Fig. 8E). Thresholds were chosen to maximize the number of bins with exactly one TerL gene and minimize the number of bins with multiple TerL genes (Supplementary Fig. 8G). For each bin, contigs with a Pearson correlation coefficient to the bin seed <0.96 or a Euclidean distance to the seed >1.05 were removed from the bin, and added to the pool of unbinned contigs. Eventually, every bin still displaying multiple TerL genes after this refinement step were split, and all corresponding contigs added to the pool of "unbinned" contigs (Supplementary Fig. 8E).

The final set of contigs was formed by compiling (i) all contigs belonging to a viral bin, (ii) "unbinned" viral contigs (i.e. contigs affiliated to archaeal and bacterial virus and not part of any genome bin), and (iii) viral contigs identified in microbial or eukaryote virus bins (considered as "unbinned" contigs, Supplementary Fig. 8F). Within this set of contigs, all viral bins were considered as viral populations, as well as every unbinned viral contig ≥10kb, leading to a total of 15,222 epi- and mesopelagic populations, and 58 bathypelagic populations (Supplementary Fig. 1, Supplementary Table 2, and Supplementary Text). In this study, we focus only on the 15,222 epi- and mesopelagic populations, totaling 24,353 contigs. For the detection of AMGs, we added to these populations all short epi- and mesopelagic unbinned viral contigs (<10kb), adding up to a total of 298,383 contigs.

Sequence clustering and annotations

Dataset of publicly available viral genomes and genome fragments

Genomes of viruses associated with a bacterial or archaeal host were downloaded from NCBI RefSeq (1,680 sequences, v70, 05-26-2015). To complete this dataset of reference genomes, viral genomes and genome fragments available in Genbank but not in RefSeq were downloaded (July 2015) and manually curated to select only bacterial and archaeal viruses (1,017 sequences). These included viral genomes not yet added to RefSeq, as well as genome fragments from fosmid libraries generated from seawater samples[9,10]. Mycophage sequences (available from http://phagesdb.org[49]) were downloaded (July 2015) and included as well if not already in RefSeq (734 sequences). Finally, 12,498 viral genome fragments from the VirSorter Curated Dataset, identified in publicly available microbial

genome sequencing projects, were added to the database[8].

Genome (fragments) clustering through gene-content based network analysis

Proteins predicted from 14,650 large GOV contigs (≥10kb and ≥10 genes), were added to all proteins from the publicly available viral genomes and genomes fragments gathered, and compared through all-vs-all blastp, with a threshold of 10^{-5} on e-value and 50 on bit score. Protein clusters were then defined using MCL (using default parameters for clustering of proteins, similarity scores as log-transformed e-value, and 2 for MCL inflation[50]). vContact (https://bitbucket.org/MAVERICLab/vcontact) was then used to calculate a similarity score between every pair of genome and/or contigs based on the number shared of PCs between the two sequences (as in[7,8]), and then compute a MCL clustering of the genomes/contigs based on these similarity scores (thresholds of 1 on similarity score, MCL inflation of 2). The resulting viral clusters (or VCs, clusters including ≥2 contigs and/or genomes), consistent with a clustering based on whole-genome BLAST comparison, corresponded to approximately genus-level taxonomy, with rare cases closer to subfamily-level taxonomy (Extended Data Fig. 2 and Supplementary Text). A total of 1,259 viral clusters were obtained, with 867 including at least one GOV sequence. Notably, however, automatically defined VCs merely serve as a starting place for assigning viral taxonomy. Current ICTV convention for formal taxonomic consideration of these VCs would require manual comparison of genomes and genome fragments to identify signature genes, comparison of phylogenetic signals, and ideally observation of morphological features of corresponding viruses, although this process is currently being reviewed as advanced computational analytics and genome datasets, such as those presented here, are being developed.

Viral contigs annotation

A functional annotation of all GOV predicted proteins was based on a comparison to the PFAM domain database (v27[51]) with HmmSearch[52] (threshold of 30 on bit score and 1e-3 on e-value), and additional putative structural proteins were identified through a BLAST comparison to protein clusters detected in viral metaproteomics dataset[53]. This metaproteomics dataset led to the annotation of 13,547 hypothetical proteins lacking a PFAM annotation. A taxonomic annotation was performed based on a blastp of the predicted proteins against proteins from archaeal and bacterial viruses from NCBI RefSeq and Genbank (threshold of 50 on bit score and 10^{-3} on e-value).

VCs were affiliated based on isolate genome members, when available. When multiple isolates were included in the VC, the VC was affiliated to the corresponding subfamily or genus of these isolates (excluding all "unclassified" cases). This was the case for VC_2 (T4 subfamily[14,15]), and VC_9 (*T7virus*[16]). When only one or a handful of affiliated isolate genomes were included in the VC and lacked genus-level classification, a candidate name was derived from the isolate (if several isolates, from the first one isolated). This was the case for VC_5 (*Cbaphi381virus*[54]), VC_12 (*P12024virus*[55]), VC_14 (*MED4-117virus*), VC_19 (*HMO-2011virus*[56]), VC_31 (*RM378virus*[57]), VC_36 (*GBK2virus*[58]), VC_47 (*Cbaphi142virus*[54]) , and VC_277 (*vB_RglS_P106Bvirus*[59]). Otherwise, VCs were considered as "new VCs".

"Phage proteomic tree" (i.e. "whole-genome comparison tree") computation and visualization

All publicly available complete genomes (see above), all complete (circular) and near-complete (extrachromosomal genome fragment >50kb with a terminase) from the VirSorter Curated Dataset, and all complete and near-complete GOV contigs were compared to generate a phage proteomic tree, as previously described[9,60]. Briefly, a proteomic similarity score was calculated for each pair of genome based on a all-vs-all tblastx similarity as the sum of bit scores of significant hits between two genomes (e-value ≤ 0.001, bit score ≥30, identity percentage ≥ 30). To normalize for different genome sizes, each genome was also compared to itself to generate a self-score, and the distance between two different genomes was calculated as a Dice coefficient (as in[9]), i.e. for two genomes A and B with a

proteomic similarity score of AB, the corresponding distance d would be 1-(2*AB)/(AA+BB), with AA and BB being the self-score of genomes A and B respectively. For clarity, the tree displayed in Extended Data Fig. 2 only include non-GOV sequences found in a VC with GOV sequence(s) or within a distance <0.5 to a GOV sequence, adding for a total of 1,522 reference sequences. iTOL[61,62] was used to visualize and display the tree.

Distribution and relative abundance of viral populations and VCs

Detection and estimation of abundance for viral contigs and populations

The presence and relative abundance of a viral contig in a sample were determined based on the mapping of HQ reads to the contig sequences, computed with Bowtie 2 (options --sensitive, -X 2000, and --non-deterministic, default parameters otherwise[42]), as previously described[4]. A contig was considered as detected in a metagenome if more than 75% of its length was covered by aligned reads derived from the corresponding sample. A normalized coverage for the contig was then computed as the average contig coverage (i.e. number of nucleotides mapped to the contig divided by the contig length) normalized by the total number of bp sequenced in this sample. The detection and relative abundance of a viral population was based on the coverage of its contigs: a population was considered as detected in a sample if more than 75% of its cumulated length was covered, and its normalized coverage was computed as the average normalized coverage of its contigs.

Relative abundance of VCs

The relative abundance of VCs was calculated based on the coverage of its members within the 15,222 viral populations identified. If a population included contigs all linked to the same VC, or linked to a single VC except for unclustered (because too short) contigs, this population coverage was added to the total of the corresponding VC. In the rare cases where the link between population and VC was ambiguous because different contigs within a population pointed toward different VCs (n=475, i.e. 3.1% of the populations), the population coverage was equally split between these VCs. Finally, if no contig in the population belonged to any VC (n=2,605, 17% of the populations), the population coverage was added to the "unclustered" category. Eventually, for each sample, the cumulated coverage of a VC was normalized by the total coverage of all populations to calculate a relative abundance of the VC among viral populations.

The selection of abundant VCs within a sample was based on the contribution of the VC to the sample diversity as measured by the Simpson index. For each sample, the overall Simpson index was first calculated with all VCs. Then, VCs were sorted by decreasing relative abundance and progressively added to a new calculation of the Simpson index. VCs considered as abundant were the ones which, once cumulated, represented 80% of the sample diversity (i.e. a Simpson index greater or equal to 80% of the sample total Simpson index, Extended Data Fig. 1C). The 38 VCs identified as abundant in at least 2 different stations were selected as "recurrently abundant VCs in the GOV dataset" (Fig. 2 and Extended Data Fig. 3).

Host prediction and diversity

Three different approaches were used to link viral contigs and putative host genomes: blastn similarity, CRISPR spacer similarity, and tetranucleotide frequencies similarities. An overview of the contigs generation process is provided in Supplementary Fig. 8, and an extended discussion about the efficiency and raw results of these host prediction methods is provided in Supplementary Text, Supplementary Table 4, and ref. [63]. A list of all host predictions by viral sequence is available in Supplementary Table 5.

Generation of host database

A genome database of putative hosts for the epi- and mesopelagic GOV viruses was generated,

including all archaea and bacteria genomes annotated as "marine" from NCBI RefSeq and WGS (both times only sequences ≥5kb, 184,663 sequences from 4,452 genomes, downloaded in August 2015), and all contigs ≥5kb from the 139 *Tara* Oceans microbial metagenomes corresponding to the bacteria and archaea size fraction (791,373 sequences)[18]. For these microbial metagenomic contigs, a first blastn was computed to compare them to all GOV contigs, and exclude from the putative host dataset all metagenomic contigs with a significant similarity to a viral GOV sequence (thresholds of 50 on bit score, 0.001 on e-value, and 70% on identity percentage) on ≥90% of their length, as these are likely sequences of viral origin sequenced in the bacteria and archaea size fraction (these represented 2.2% of the contigs in the assembled microbial metagenomes). The taxonomic affiliation of NCBI genomes was taken from the NCBI taxonomy. For *Tara* Oceans contigs, a last common ancestor (LCA) affiliation was generated for each contig based on genes affiliation[18], if 3 genes or more on the contig were affiliated.

BLAST-based identification of sequence similarity between viral contigs and host genome

All GOV viral contigs were compared to all archaeal and bacterial genomes and genome fragments with a blastn (threshold of 50 on bit score and 0.001 on e-value), to identify regions of similarity between a viral contig and a microbial genome, indicative of a prophage integration or horizontal gene transfer[63]. A host prediction was made when (i) a NCBI genomes displayed a region similar to a GOV viral contig ≥5kb at ≥70% id, or (ii) when a *Tara* Oceans microbial metagenomic contig (≥5kb) displayed a region similar to a GOV viral contig ≥2.5kb at ≥70% id.

Matches between GOV viral contigs and CRISPR spacers.

CRISPR arrays were predicted for all putative host genomes and genome fragments (NCBI microbial genomes and *Tara* Oceans microbial metagenomic contigs) with MetaCRT[64,65]. CRISPR spacers were extracted, and all spacers with ambiguous bases or low complexity (i.e. consisting of 4 to 6 bp repeat motifs) were removed. All remaining spacers were matched to viral contigs with fuzznuc[66], with no mismatches allowed, which although rarely observed yields highly accurate host predictions[63](Supplementary Table 4).

Nucleotide composition similarity: comparison of tetranucleotide frequency

Bacterial and archaeal viruses tend to have a genome composition close to the genome composition of their host, a signal that can be used to predict viral-host pairs[8,63,67]. Here, canonical tetranucleotide frequencies were observed for all viral and host sequences using Jellyfish[68], and mean absolute error (i.e. average of absolute differences) between tetranucleotide frequency vectors were computed with in-house Perl and Python scripts for each pair of viral and host sequence as in ref. [8]. A GOV viral contig was then assigned to the closest sequence (i.e. lowest distance d) from the pool of NCBI genomes if $d<0.001$ (because both the tetranucleotide frequency signal and the taxonomic affiliation of these complete genomes are more robust than for metagenomic contigs), and otherwise assigned to the closest (i.e. lowest distance) *Tara* Oceans microbial contig if $d<0.001$.

Summarizing host prediction at the VC level

Overall, 3,675 GOV contigs could be linked to a putative host group among the 24,353 GOV contigs associated with an epi- or mesopelagic viral population. To summarize these affiliations at the VC level, a Poisson distribution was used to estimate the number of expected false positive associations for each VC – host group combination based on (i) the global probability of obtaining a host prediction across all pairs of viral and host sequences tested and for all methods (5.8×10^{-08}), (ii) the number of potential predictions generated for the VC, corresponding to 3 times the number of sequences in the VC (to take into account the three methods), and (iii) the number of sequences from the host group in the database (Supplementary Figure 2). By comparing the number of links observed between a VC and a

host group to this expected value, which takes into account the bias in database (i.e. some host groups will be over- or under-represented in our set of archaeal and bacterial genomes and genome fragments) and the bias linked to the variable number of sequences in VCs, we can determine if the number of associations observed for any VC – host group combination is likely to be due to chance alone (and calculate the associated p-value).

Microbial community diversity and richness indexes

Diversity and richness indexes for putative host populations were based on the OTU abundance matrix generated from the analysis of miTAGs in *Tara* Oceans microbial metagenomes[18]. These indexes were computed for each host group at the same taxonomic level as the host prediction, i.e. the phylum level except for Proteobacteria where the class level is used. The R package vegan[69] was used to estimate for each group (i) a global Chao index (i.e. including all OTUs from all samples) through the function estaccumR, (ii) a sample-by-sample Chao index with the function estimateR, and (iii) Sorensen indexes between all pairs of samples with the function betadiver. Diversity indexes presented in Extended Data Fig 4 are based on epipelagic samples only, as the 38 VCs identified as abundant were mostly retrieved in epipelagic samples. Candidate division OP1 was excluded from this analysis because no OTU affiliated to this phylum was identified.

Identification and annotation of putative AMGs

Detection of AMGs

Predicted proteins from all GOV viral contigs were compared to the PFAM domain database (hmmsearch[52], threshold of 40 on bit score and 0.001 on e-value), and all PFAM domains detected were classified into 8 categories: "structural", "DNA replication, recombination, repair, nucleotide metabolism", "transcription, translation, protein synthesis", "lysis", "membrane transport, membrane-associated", "metabolism", "other", and "unknown" (as in ref. [20]). Four AMGs (i.e. similar to a domain from the "metabolism" category) were then selected for further study because of their central role in sulfur (*dsr*C and *sox*YZ) or nitrogen (P-II, *amo*C) cycle, and the fact that these had never been detected in a surface ocean viral genome so far (*dsrC/tusE*-like genes have been detected in deep water viruses[11,21]). To evaluate if an AMG was "known", a list of PFAM domain detected in NCBI RefSeqVirus and Environmental Phages was computed based on a similar hmmsearch comparison (threshold of 40 on bit score and 0.001 on e-value), and augmented by manual annotation of AMGs from[20,70]. These corresponded for the most part to photosynthesis and carbon metabolism AMGs previously described in cyanophages[71–75]. The complete list of PFAM domains detected in GOV viral contigs is available as Supplementary Table 6.

Phylogenetic tree generation and contigs map comparison

Sequences similar to these AMGs were recruited from the *Tara* Oceans microbial metagenomes[18] based on a blastp of all predicted proteins from microbial metagenome to the viral AMGs identified (threshold of 100 on bit score, 10^{-5} on e-value, except for P-II where a threshold of 170 on bit score was used because of the high number of sequences recruited). The viral AMG sequences were also compared to NCBI nr database (blastp, threshold of 50 on bit score and 10^{-3} on e-value) to recruit relevant reference sequences (up to 20 for each viral AMG sequence). These sets of viral AMGs and related protein sequences were then aligned with Muscle[76], the alignment manually curated to remove poorly aligned positions with Jalview[77], and two trees were computed from the same curated alignment: a maximum-likelihood tree with FastTree (v2.7.1, model WAG, other parameters set to default[78]) and a bayesian tree with MrBayes (v3.2.5, mixed evolution models, other parameters set to default, 2 MCMC chains were run until the average standard deviation of split frequencies was <0.015, relative burn-in of 25% used to generate the consensus tree[79]). In all cases except AmoC, the mixed model used by MrBayes was 100% WAG, confirming that this model was well suited for archaeal and

bacterial virus protein trees. Manual inspection revealed only minor differences between each pair of trees, so an SH test was used to determine which tree best fitted the sequence alignment, using the R library phangorn[80]. Itol[61] was used to visualize and display these trees, in which branches with supports <40% were collapsed. Annotated interactive trees are available online at http://itol.embl.de/shared/Siroux. Contigs map comparison were generated with Easyfig[81], following the same method as for the VCs (see Supplementary Information).

Functional characterization of putative AMGs

Conserved motifs were identified on the different AMGs based on the literature: *dsr*C conserved motifs were obtained from ref. [24], *sox*YZ conserved residues were identified from the PFAM domains PF13501 and PF08770, and P-II conserved motifs from PROSITE documentation PDOC00439. A 3D structure could also be predicted for P-II AMGs by I-TASSER[82] (default parameters), the quality of these predictions being confirmed with ProSA web server[83]. To further confirm the functionality of these genes, selective constraint on these AMGs was evaluated through pN/pS calculation, as in ref. [84]. Briefly, synonymous and non-synonymous SNPs were observed in each AMG, and compared to expected ratio of synonymous and non-synonymous SNPs under a neutral evolution model for this genes. The interpretation of pN/pS is similar as for dN/dS analyses, with the operation of purifying selection leading to pN/pS values < 1. Finally, AMG transcripts were searched in metatranscriptomic datasets generated through the *Tara* Oceans consortium (ENA Id ERS1092158, ERS488920, and ERS494518). For generating these metatranscriptomes, bacterial rRNA depletion was carried out on 240–500 ng total RNA using Ribo-Zero Magnetic Kit for Bacteria (Epicentre, Madison, WI) for 0.2–1.6 and 0.22–3µm filters. The Ribo-Zero depletion protocol was modified to be adapted to low RNA input amounts[85]. Depleted RNA was used to synthetize cDNA with SMARTer Stranded RNA-Seq Kit (Clontech, Mountain View, CA)[85]. Metatranscriptomic libraries were quantified by qPCR using the KAPA Library Quantification Kit for Illumina Libraries (KapaBiosystems, Wilmington, MA) and library profiles were assessed using the DNA High Sensitivity LabChip kit on an Agilent Bioanalyzer (Agilent Technologies, Santa Clara, CA). Libraries were sequenced on Illumina HiSeq2000 instrument (Illumina, San Diego,CA) using 100 base-length read chemistry in a paired-end mode. High quality reads were then mapped to viral contigs containing *dsrC*, *soxYZ,* P-II, or *amo*C genes with SOAPdenovo2[43] within MOCAT[40] (options *screen* and *filter* with length and identity cutoffs of 45 and 95%, respectively, and paired-end filtering set to *yes*), and coverage was defined for each gene as the number of bp mapped divided by gene length (including only reads mapped to the predicted coding strand).

Distribution of AMGs and association with geochemical metadata

The distribution and relative abundance of AMGs was based on the read mapping and normalized coverage of the contig including the AMG. To get a range of temperature and nutrient concentrations for the widespread AMGs (detected in >5 stations) that takes into account both the samples in which these AMGs were detected and the differences in normalized coverage, a set of samples was selected through a weighted random drawing replacement, with the weight of each sample corresponding to the AMG's normalized coverage. That way, a range of temperature or nutrient concentration values associated with the AMG's distribution and abundance could be generated for each AMG and each environmental parameter tested. The number of samples randomly selected for each AMG was the same as the total number of samples for which a value of this parameter was available.

Code and data availability

Scripts used in this manuscript are available on the Sullivan lab bitbucket under project "GOV_Ecogenomics" (http://bitbucket.org/MAVERICLab/gov_ecogenomics/overview). Scripts used in the assessment of microbial diversity are gathered in the directory "Host_diversity", the ones used

for host predictions are in "Host_prediction", and the scripts used to identify abuntant VCs are in "Virus_clusters_prevalence". All raw reads are available through ENA (*Tara* Oceans) or JGI (Malaspina) using the dataset identifiers listed in Supplementary Table 1. Processed data are available through iVirus (http://mirrors.iplantcollaborative.org/browse/iplant/home/shared/ivirus/GOV/), including all sequences from assembled contigs, list of viral populations and associated annotated sequences as genbank files, viral clusters composition and characteristics, map comparisons of genomes and contigs of the 38 abundant VCs, and host predictions for viral contigs.

References

1. Falkowski, P. G., Fenchel, T. & Delong, E. F. The Microbial Engines That Drive Earth's Biogeochemical Cycles. *Science* **320,** 1034–9 (2008).

2. Rohwer, F. & Thurber, R. V. Viruses manipulate the marine environment. *Nature* **459,** 207–212 (2009).

3. Brum, J. R. & Sullivan, M. B. Rising to the challenge: accelerated pace of discovery transforms marine virology. *Nat. Rev. Microbiol.* **13,** 147–59 (2015).

4. Brum, J. *et al.* Patterns and ecological drivers of ocean viral communities. *Science* **348,** 1261498–1–10 (2015).

5. Karsenti, E. *et al.* A holistic approach to marine eco-systems biology. *PLoS Biol.* **9,** e1001177 (2011).

6. Duarte, C. M. Seafaring in the 21st Century : The Malaspina 2010 Circumnavigation Expedition. *Limnology and Oceanography Bulletin* **24**, 11–14 (2015).

7. Lima-Mendez, G., Van Helden, J., Toussaint, A. & Leplae, R. Reticulate representation of evolutionary and functional relationships between phage genomes. *Mol. Biol. Evol.* **25,** 762–77 (2008).

8. Roux, S., Hallam, S. J., Woyke, T. & Sullivan, M. B. Viral dark matter and virus-host interactions resolved from publicly available microbial genomes. *Elife* **4,** 1–20 (2015).

9. Mizuno, C. M., Rodriguez-Valera, F., Kimes, N. E. & Ghai, R. Expanding the marine virosphere using metagenomics. *PLoS Genet.* **9,** e1003987 (2013).

10. Chow, C.-E. T., Winget, D. M., White, R. a., Hallam, S. J. & Suttle, C. a. Combining genomic sequencing methods to explore viral diversity and reveal potential virus-host interactions. *Front. Microbiol.* **6,** 1–15 (2015).

11. Roux, S. *et al.* Ecology and evolution of viruses infecting uncultivated SUP05 bacteria as revealed by single-cell- and meta- genomics. *Elife* **3,** 1–20 (2014).

12. Dutilh, B. E. *et al.* A highly abundant bacteriophage discovered in the unknown sequences of human faecal metagenomes. *Nat. Commun.* **5,** 1–11 (2014).

13. Albertsen, M. *et al.* Genome sequences of rare, uncultured bacteria obtained by differential coverage binning of multiple metagenomes. *Nat. Biotechnol.* **31,** 533–8 (2013).

14. Sullivan, M. B. *et al.* Genomic analysis of oceanic cyanobacterial myoviruses compared with T4-

like myoviruses from diverse hosts and environments. *Environ. Microbiol.* **12,** 3035–56 (2010).

15. Zhao, Y. *et al.* Abundant SAR11 viruses in the ocean. *Nature* **494,** 357–360 (2013).

16. Labrie, S. J. *et al.* Genomes of marine cyanopodoviruses reveal multiple origins of diversity. *Environ. Microbiol.* **15,** 1356–76 (2013).

17. Andersson, A. F. & Banfield, J. F. Virus population dynamics and acquired virus resistance in natural microbial communities. *Science* **320,** 1047–50 (2008).

18. Sunagawa, S. *et al.* Structure and function of the global ocean microbiome. *Science* **348,** 1–10 (2015).

19. Flores, C. O., Valverde, S. & Weitz, J. S. Multi-scale structure and geographic drivers of cross-infection within marine bacteria and phages. *ISME J.* **7,** 520–32 (2013).

20. Hurwitz, B. L., Brum, J. R. & Sullivan, M. B. Depth-stratified functional and taxonomic niche specialization in the "core" and "flexible" Pacific Ocean Virome. *ISME J.* **9,** 472–84 (2015).

21. Anantharaman, K. *et al.* Sulfur Oxidation Genes in Diverse Deep-Sea Viruses. *Science2* **344,** 757–760 (2014).

22. Friedrich, C. G., Bardischewsky, F., Rother, D., Quentmeier, A. & Fischer, J. Prokaryotic sulfur oxidation. *Curr. Opin. Microbiol.* **8,** 253–9 (2005).

23. Santos, A. A. *et al.* A protein trisulfide couples dissimilatory sulfate reduction to energy conservation. *Science* **350,** 1541–1546 (2015).

24. Venceslau, S. S., Stockdreher, Y., Dahl, C. & Pereira, I. A. C. The "bacterial heterodisulfide" DsrC is a key protein in dissimilatory sulfur metabolism. *Biochim. Biophys. Acta* **1837,** 1148–64 (2014).

25. Dahl, C., Franz, B., Hensen, D., Kesselheim, A. & Zigann, R. Sulfite oxidation in the purple sulfur bacterium Allochromatium vinosum: identification of SoeABC as a major player and relevance of SoxYZ in the process. *Microbiology* **159,** 2626–38 (2013).

26. Huergo, L. F., Chandra, G. & Merrick, M. P(II) signal transduction proteins: nitrogen regulation and beyond. *FEMS Microbiol. Rev.* **37,** 251–83 (2013).

27. Stahl, D. A. & de la Torre, J. R. Physiology and diversity of ammonia-oxidizing archaea. *Annu. Rev. Microbiol.* **66,** 83–101 (2012).

28. Loy, A. *et al.* Reverse dissimilatory sulfite reductase as phylogenetic marker for a subgroup of sulfur-oxidizing prokaryotes. *Environ. Microbiol.* **11,** 289–99 (2009).

29. Pester, M., Schleper, C. & Wagner, M. The Thaumarchaeota: an emerging view of their phylogeny and ecophysiology. *Curr. Opin. Microbiol.* **14,** 300–6 (2011).

30. Weitz, J. S. *et al.* A multitrophic model to quantify the effects of marine viruses on microbial food webs and ecosystem processes. *ISME J.* **9,** 1352–1364 (2015).

31. Arcondéguy, T., Jack, R. & Merrick, M. P II Signal Transduction Proteins, Pivotal Players in Microbial Nitrogen Control. *Microbiol. Mol. Biol. Rev.* **65,** 80–105 (2001).

References: Methods section

32. Pesant, S. *et al.* Open science resources for the discovery and analysis of Tara Oceans data. *Sci. Data* **2,** 150023 (2015).

33. John, S. G. *et al.* A simple and efficient method for concentration of ocean viruses by chemical flocculation. *Environ. Microbiol. Rep.* **3,** 195–202 (2011).

34. Hurwitz, B. L., Deng, L., Poulos, B. T. & Sullivan, M. B. Evaluation of methods to concentrate and purify ocean virus communities through comparative, replicated metagenomics. *Environ. Microbiol.* **15,** 1428 – 1440 (2012).

35. Aminot, A., Kérouel, R. & Coverly, S. in *Pract. Guidel. Anal. Seawater* 143–176 (2009).

36. Tara Oceans Consortium & Tara Oceans Expedition. Registry of all samples from the Tara Oceans Expedition (2009-2013). (2015). doi:10.1594/PANGAEA.842197

37. Tara Oceans Consortium & Tara Oceans Expedition. Environmental context of all samples from the Tara Oceans Expedition (2009-2013). (2015). doi:10.1594/PANGAEA.853810

38. Tara Oceans Consortium & Tara Oceans Expedition. Biodiversity context of all samples from the Tara Oceans Expedition (2009-2013). (2015). doi:10.1594/PANGAEA.853809

39. Salazar, G. *et al.* Global diversity and biogeography of deep-sea pelagic prokaryotes. *ISME J.* **10**, 596–608 (2016). doi:10.1038/ismej.2015.137

40. Kultima, J. R. *et al.* MOCAT: a metagenomics assembly and gene prediction toolkit. *PLoS One* **7,** e47656 (2012).

41. Peng, Y., Leung, H. C. M., Yiu, S. M. & Chin, F. Y. L. IDBA-UD: a de novo assembler for single-cell and metagenomic sequencing data with highly uneven depth. *Bioinformatics* **28,** 1420–1428 (2012).

42. Langmead, B. & Salzberg, S. L. Fast gapped-read alignment with Bowtie 2. *Nat. Methods* **9,** 357–9 (2012).

43. Luo, R. *et al.* SOAPdenovo2 : an empirically improved memory-efficient short-read de novo assembler. *Gigascience* **1,** 1–6 (2012).

44. Li, W. & Godzik, A. Cd-hit: a fast program for clustering and comparing large sets of protein or nucleotide sequences. *Bioinformatics* **22,** 1658–9 (2006).

45. Kang, D. D., Froula, J., Egan, R. & Wang, Z. MetaBAT, an efficient tool for accurately reconstructing single genomes from complex microbial communities. *PeerJ* **3,** e1165 (2015).

718 46. Mavromatis, K., Ivanova, N., Barry, K. & Shapiro, H. Use of simulated data sets to evaluate the
719 fidelity of metagenomic processing methods. *Nat. Methods* **4,** 495–500 (2007).

720 47. Roux, S., Krupovic, M., Debroas, D., Forterre, P. & Enault, F. Assessment of viral community
721 functional potential from viral metagenomes may be hampered by contamination with cellular
722 sequences. *Open Biol.* **3,** 130160 (2013).

723 48. Roux, S., Enault, F., Hurwitz, B. L. & Sullivan, M. B. VirSorter: mining viral signal from microbial
724 genomic data. *PeerJ* **3,** e985 (2015).

725 49. Pope, W. H. *et al.* Whole genome comparison of a large collection of mycobacteriophages reveals a
726 continuum of phage genetic diversity. *Elife* **4,** (2015).

727 50. Enright, A. J., Van Dongen, S. & Ouzounis, C. A. An efficient algorithm for large-scale detection of
728 protein families. *Nucleic Acids Res.* **30,** 1575–84 (2002).

729 51. Finn, R. D. *et al.* Pfam: the protein families database. *Nucleic Acids Res.* **42,** D222–30 (2014).

730 52. Eddy, S. R. Accelerated Profile HMM Searches. *PLoS Comput. Biol.* **7,** e1002195 (2011).

731 53. Brum, J. R. *et al.* Illuminating structural proteins in viral "dark matter" with metaproteomics. *Proc.*
732 *Natl. Acad. Sci. U. S. A.* **113,** 2436-2441 (2016).

733 54. Holmfeldt, K. *et al.* Twelve previously unknown phage genera are ubiquitous in the global oceans.
734 *Proc. Natl. Acad. Sci. U. S. A.* **110,** 12798–12803 (2013).

735 55. Kang, I., Jang, H. & Cho, J.-C. Complete genome sequences of two Persicivirga bacteriophages,
736 P12024S and P12024L. *J. Virol.* **86,** 8907–8 (2012).

737 56. Kang, I., Oh, H.-M., Kang, D. & Cho, J.-C. Genome of a SAR116 bacteriophage shows the
738 prevalence of this phage type in the oceans. *Proc. Natl. Acad. Sci. U. S. A.* **110,** 12343–8 (2013).

739 57. Hjorleifsdottir, S., Aevarsson, A., Hreggvidsson, G. O., Fridjonsson, O. H. & Kristjansson, J. K.
740 Isolation, growth and genome of the Rhodothermus RM378 thermophilic bacteriophage.
741 *Extremophiles* **18,** 261–70 (2014).

742 58. Marks, T. J. & Hamilton, P. T. Characterization of a thermophilic bacteriophage of Geobacillus
743 kaustophilus. *Arch. Virol.* **159,** 2771–5 (2014).

744 59. Halmillawewa, A. P., Restrepo-Córdoba, M., Yost, C. K. & Hynes, M. F. Genomic and phenotypic
745 characterization of Rhizobium gallicum phage vB_RglS_P106B. *Microbiology* **161,** 611–20
746 (2015).

747 60. Rohwer, F. & Edwards, R. The Phage Proteomic Tree : a Genome-Based Taxonomy for Phage. *J.*
748 *Bacteriol.* **184,** 4529–4535 (2002).

749 61. Letunic, I. & Bork, P. Interactive Tree Of Life (iTOL): an online tool for phylogenetic tree display
750 and annotation. *Bioinformatics* **23,** 127–128 (2007).

751 62. Letunic, I. & Bork, P. Interactive Tree Of Life v2: online annotation and display of phylogenetic

trees made easy. *Nucleic Acids Res.* **39,** W475–8 (2011).

63. Edwards, R. A., McNair, K., Faust, K., Raes, J. & Dutilh, B. E. Computational approaches to predict bacteriophage-host relationships. *FEMS Microbiol. Rev.* **40,** 258-272 (2015).

64. Bland, C. *et al.* CRISPR recognition tool (CRT): a tool for automatic detection of clustered regularly interspaced palindromic repeats. *BMC Bioinformatics* **8,** 209 (2007).

65. Rho, M., Wu, Y.-W., Tang, H., Doak, T. G. & Ye, Y. Diverse CRISPRs Evolving in Human Microbiomes. *PLoS Genet.* **8,** e1002441 (2012).

66. Rice, P., Longden, I. & Bleasby, a. EMBOSS: the European Molecular Biology Open Software Suite. *Trends Genet.* **16,** 276–7 (2000).

67. Ogilvie, L. a *et al.* Genome signature-based dissection of human gut metagenomes to extract subliminal viral sequences. *Nat. Commun.* **4,** 2420 (2013).

68. Marçais, G. & Kingsford, C. A fast, lock-free approach for efficient parallel counting of occurrences of k-mers. *Bioinformatics* **27,** 764–70 (2011).

69. Oksanen, J. *et al. The vegan Package*. (2016).

70. Sharon, I. *et al.* Comparative metagenomics of microbial traits within oceanic viral communities. *ISME J.* **5,** 1178–90 (2011).

71. Thompson, L. R. *et al.* Phage auxiliary metabolic genes and the redirection of cyanobacterial host carbon metabolism. *Proc. Natl. Acad. Sci. U. S. A.* **108,** E757–64 (2011).

72. Dammeyer, T., Bagby, S. C., Sullivan, M. B., Chisholm, S. W. & Frankenberg-Dinkel, N. Efficient phage-mediated pigment biosynthesis in oceanic cyanobacteria. *Curr. Biol.* **18,** 442–8 (2008).

73. Lindell, D., Jaffe, J. D., Johnson, Z. I., Church, G. M. & Chisholm, S. W. Photosynthesis genes in marine viruses yield proteins during host infection. *Nature* **438,** 86–9 (2005).

74. Lindell, D. *et al.* Genome-wide expression dynamics of a marine virus and host reveal features of co-evolution. *Nature* **449,** 83–6 (2007).

75. Sullivan, M. B. *et al.* Prevalence and Evolution of Core Photosystem II Genes in Marine Cyanobacterial Viruses and Their Hosts. *PLoS Biol.* **4,** e234 (2006).

76. Edgar, R. C. MUSCLE: a multiple sequence alignment method with reduced time and space complexity. *BMC Bioinformatics* **5,** 113 (2004).

77. Waterhouse, A. M., Procter, J. B., Martin, D. M. A., Clamp, M. & Barton, G. J. Jalview Version 2--a multiple sequence alignment editor and analysis workbench. *Bioinformatics* **25,** 1189–1191 (2009).

78. Price, M. N., Dehal, P. S. & Arkin, A. P. FastTree 2--approximately maximum-likelihood trees for large alignments. *PLoS One* **5,** e9490 (2010).

79. Huelsenbeck, J. P. & Ronquist, F. MRBAYES: Bayesian inference of phylogenetic trees. *Bioinformatics* **17,** 754–755 (2001).

80. Schliep, K. P. phangorn: phylogenetic analysis in R. *Bioinformatics* **27,** 592–3 (2011).

81. Sullivan, M. J., Petty, N. K. & Beatson, S. A. Easyfig: a genome comparison visualizer. *Bioinformatics* **27,** 1009–10 (2011).

82. Roy, A., Kucukural, A. & Zhang, Y. I-TASSER: a unified platform for automated protein structure and function prediction. *Nat. Protoc.* **5,** 725–38 (2010).

83. Wiederstein, M. & Sippl, M. J. ProSA-web: interactive web service for the recognition of errors in three-dimensional structures of proteins. *Nucleic Acids Res.* **35,** W407–10 (2007).

84. Schloissnig, S. *et al.* Genomic variation landscape of the human gut microbiome. *Nature* **493,** 45–50 (2013).

85. Alberti, A. *et al.* Comparison of library preparation methods reveals their impact on interpretation of metatranscriptomic data. *BMC Genomics* **15,** 912 (2014).

Acknowledgements

We thank Joshua Weitz for advice on statistics, Claus Pelikan for help with the DsrAB phylogenetic tree, Christiane Dahl for valuable discussion regarding DsrC function, and members of the Sullivan and Rich labs for suggestions and comments on this manuscript. We acknowledge support from UA high-performance computing and the Ohio Supercomputer Center. Sponsors and support for *Tara* Oceans and Malaspina expeditions are listed in the Supplementary Information. This viral research was funded by a National Science Foundation grant (#1536989) and Gordon and Betty Moore Foundation grants (#3790, #2631) to MBS, and the French Ministry of Research and Government through the "Investissements d'Avenir" program OCEANOMICS (ANR-11-BTBR-0008). Virus researchers were partially supported by the Water, Environmental and Energy Solutions Initiative and the Ecosystem Genomics Institute (SR), the Netherlands Organization for Scientific Research Vidi grant 864.14.004 and CAPES/BRASIL (BED), and the Austrian Science Fund (project P25111-B22, AL). The authors declare that all data reported herein are fully and freely available from the date of publication, with no restrictions, at EBI, PANGAEA, and iVirus (see Methods and Supplementary Table 1), and that all of the samples, analyses, publications, and ownership of data are free from legal entanglement or restriction of any sort by the nations in whose waters *Tara* Oceans expedition sampled in. All authors approved the final manuscript. This article is contribution number 43 of the *Tara* Oceans Expedition.

Consortia

Tara Oceans Consortium Coordinators

A list of authors and affiliations appears in the Supplementary Information.

Author Contributions

S.R., and M.B.S. designed the study. C.D., M.P., and Sa.S., contributed extensively to sampling collection. S.K-L. managed the logistic of the *Tara* Oceans project. B.T.P., N.S. and E.L. performed the viral-specific processing of the samples. J.P., C.C., A.A., and P.W. led the sequencing of viral samples. S.R., S.S. and B.E.D. led the assembly of raw data. S.R., S.S., M.B.D. and M.B.S. analyzed the genomic diversity data. S.R., A.L., J.R.B. and M.B.S. analyzed the AMGs data. S.R., J.R.B., B.E.D, S.S., M.B.D., A.L., S.P., P.B., S.G.A., C.D., J.M.G., D.V. and M.B.S. provided constructive comments,

revised and edited the manuscript. *Tara* Oceans coordinators provided creative environment and constructive criticism throughout the study. All authors discussed the results and commented on the manuscript.

Competing financial interests

The authors declare no competing financial interests.

Author Information

Reprints and permissions information is available at www.nature.com/reprints. Correspondence and requests for materials should be addressed to mbsulli@gmail.com.

Figure legends

Figure 1: Composition of the Global Ocean Viromes (GOV) dataset. A. Size of viral contigs (x-axis) and cumulative coverage across the GOV dataset (y-axis). Contigs corresponding to complete (345 contigs) or near-complete genomes (425 contigs) are indicated. For clarity, only contigs associated with a viral population (24,412 contigs) are displayed. **B.** Distribution of all viral clusters (VCs) according to the origin of their members. Viral genomes (or fragments) in a VC can originate from isolate viral genomes, the VirSorter Curated Dataset[8] (viral genomes identified *in silico* from microbial genomes), environmental viral genomes and genome fragments (e.g. from fosmid libraries), or the GOV dataset. VCs including at least one GOV sequence and further analyzed in this study are highlighted in bold.

Figure 2: Characterization of the dominant oceanic viral clusters (VCs). **A.** Distribution and abundance of the 38 recurrently abundant VCs according to the total number of stations in which members of the VC were detected (x-axis), and the number of samples in which the VC was detected in the abundant fraction (y-axis). "Known viruses" are VCs with ICTV-classified reference sequences, "Unclassified reference(s)" are VCs with isolate genomes lacking ICTV classification, and "New VCs" are composed solely of environmental sequences. **B.** GOV samples with their most abundant VC mapped to station locations. Samples are stacked vertically when multiple depths are available, with a horizontal line separating epipelagic from mesopelagic layers. Map modified with permission from N. Le Bescot, EPEP, CNRS Roscoff. **C.** Summary of the 4 globally abundant VCs affiliation, origin of VC members (Env: environmental viral sequences), estimated genome size, predicted host range, and distribution (relative abundance are indicated as % of the viral populations identified). The abundant epipelagic microbial groups (representing >1% of the microbial OTUs abundance of epipelagic samples) are highlighted in bold; Alphaproteob.-Alphaproteobacteria, Betaproteob.-Betaproteobacteria, Deinococcus-Th.-Deinococcus-Thermus, Deltaproteob.-Deltaproteobacteria, Gammaproteob.-Gammaproteobacteria, Cand div OP1-Candidate division OP1. Oceanic basins are indicated for VCs distributions; Med. Sea-Mediterranean Sea.

Figure 3: Characterization and distribution of viral Auxiliary Metabolic Genes (AMGs) involved in sulfur and nitrogen cycles. Schematics for (**A**) microbial sulfur oxidation pathways involving the two main gene clusters (*dsr* and *sox*) and (**B**) the central role of the P-II protein in cell regulation (adapted from[26,31]). AMG color outlines indicate their viral taxonomic affiliation. Ammonium transporters detected next to viral P-II are highlighted with a dashed outline. **C.** Distribution of viral AMG clades, with mesopelagic samples highlighted in green, and geographically restricted clades outlined. **D.** Temperature and nutrient conditions for which widespread epipelagic AMGs tend to be most abundant. For each environmental parameter, the range across all epipelagic samples is displayed alongside distributions representing the range of values where each AMG clade was detected, weighted

by the AMG coverage across these samples (see Extended Data Fig. 9 for underlying coverage data). Distributions significantly different from the "All Samples" distribution (two-sided KS-test) are indicated with stars. Boxes represent the first and third quartiles around the median.

Extended Data Figure 1: Accumulation curves of populations (A) and viral clusters (VCs, B) and identification of abundant VCs in GOV samples (C). A & B. Accumulation curves were computed from 50 randomly shuffled samples (blue dots), with all, epipelagic, mesopelagic, or bathypelagic subsets of the data. For each curve, the average of 50 iterations is displayed with red dots. C. Schematic of the selection process of abundant VCs. For each sample, VCs accounting for (up to) 80% of the sample diversity (as assessed by Simpson index) were considered as abundant (example for sample 125_MIX on the left). VCs detected as abundant in at least two different stations were included in the 38 VCs described in Fig. 2 and Extended Data Fig. 3.

Extended Data Figure 2: Comparison of VCs with other classification methods: phage proteomic tree and percentage of shared genes. The phage proteomic tree includes the 756 GOV complete and near-complete genomes from epi- and mesopelagic samples, and closest references from RefSeq and Environmental phages (d<0.5 to a GOV sequence or found in the same VC as a GOV sequence). Branches of monophyletic clades including more than 3 GOV and/or uncultivated marine sequences with no isolate reference are highlighted in blue. All VCs with more than 8 representatives in the tree or part of the 38 abundant VCs are indicated with coloring of the outer ring. The name and affiliation (if available) of the 38 abundant VCs are indicated next to the VC on the colored ring. VCs whose members were gathered in a single monophyletic clades are indicated with a solid black outline, while VCs for which all but one members were gathered in a single monophyletic clades are highlighted with a dashed black outline. Inset: distribution of number of shared genes estimated based on the number of shared PCs (protein clusters) for viral genome/contigs pairs either between different VCs or within VCs. On average, 73% and 39% of sequences within a VC shared more than 20% and 40% of their genes, respectively, which represent the current thresholds currently accepted for sub-family and genus designations. Similarly, 83% of sequences within a VC were consistently affiliated in the phage proteomic tree as they formed a monophyletic group including only members of the particular VC. Thus all three classification methods are largely consistent for the GOV dataset (see Supplementary Text).

Extended Data Figure 3: Summary of 34 of the 38 abundant viral clusters (VCs, the 4 other abundant VCs being the ubiquitous ones presented in Fig. 2). Predicted genome size is based on the set of isolates and circular contigs in the VC (NA corresponds to VCs without any circular contigs, or for which the relative standard deviation of estimated genome size across the different isolate(s) and/or circular contigs is greater than 15%). Host association values are based on the number of cluster members associated with each host group, the statistical significance of this number of predictions being evaluated by comparison with an expected number of associations calculated from a Poisson distribution. Host associations based on known isolates are indicated with a star (for associations based on cultivated isolates) or a dot (for associations based on the detection of a cluster member in a microbial genome from the VirSorter Curated Dataset). The abundant epipelagic microbial groups (representing >1% of the microbial OTUs abundance of epipelagic samples) are highlighted in bold. Distribution and relative abundance of VCs are based on the cumulated coverage of VC members among sample viral populations. The main oceanic basins are indicated for each set of sample, Med. Sea-Mediterranean Sea.

Extended Data Figure 4: Association between abundant viral clusters (VCs) and host group abundance and diversity A. Abundance and diversity of bacterial and archaeal host groups associated

with the 38 abundant VCs (see Fig. 2A). For each host group (phylum level, except for Proteobacteria where the class level is used), the different panels display from top to bottom (i) the number of VCs associated with this host group, (ii) the global relative abundance of this group estimated from the microbial metagenomic OTU counts, (iii) the global diversity of this group based on a Chao index computation including all *Tara* Oceans microbial metagenome samples (i.e. including both Alpha and Beta diversity), (iv) the distribution of Chao indexes by sample for this group (Alpha diversity), and (v) the average Sorensen index between pairs of samples including at least one OTU of this group (Beta diversity). OTU counts were derived from the 109 epipelagic microbial metagenomes described in[18]. **B.** Pearson correlations between host group relative abundance or diversity indexes (Global Chao, Average Chao across samples, and Average Sorensen across samples) and the number of VCs.

Extended Data Figure 5: Diversity, distribution, and genome context of *dsr*C genes in GOV contigs. A. Maximum-likelihood tree (from an amino-acid alignment) including the 11 viral DsrC and microbial sequences from microbial metagenomes and NCBI nr database. The presence of conserved C residues (named Cys-A & Cys-B, as in ref. [24]) is indicated with color circles next to each sequence or clade, and the corresponding type of DsrC-like protein is indicated by coloring the branch or clade. The microbial metagenomic contigs affiliated to uncultivated, marine sulfur-oxidizing Gammaproteobacteria (as confirmed by complementary phylogenetic analysis of DsrAB, Supplementary Fig. 7) are indicated with a star next to the sequence or clade. Viral AMG sequences are highlighted in blue, internal nodes SH-like supports are represented by proportional circles (all nodes with support < 0.40 were collapsed). Each *dsrC* AMG is associated with an abundance profile (on the right) displaying the relative abundance of the contig across the 91 epi- and mesopelagic samples (based on normalized coverage, i.e. contig coverage / Gb of metagenome). **B.** Comparison of *dsrC*-containing contigs maps. T4-like marker gene (T4 baseplate) is indicated on the maps, alongside putative AMGs (Fe-S biosyn for Iron-sulfur cluster biosynthesis, and Amt for Ammonia transporter).

Extended Data Figure 6: Diversity, distribution, and genome context of s*ox*YZ genes in GOV contigs. A. Bayesian tree (from an amino-acid alignment) including the 4 viral SoxYZ and microbial sequences from microbial metagenomes and NCBI nr database. The affiliation of microbial clades (either from the NCBI reference or from the LCA affiliation of metagenomic contigs) is indicated by coloring of the grouped clades or with a colored square next to the sequence. Viral AMG sequences are highlighted in blue, posterior probabilities are represented by proportional circles (all nodes with posterior probability < 0.40 were collapsed). Clades including sulfur-oxidation proteobacteria are indicated on the tree. Each s*ox*YZ AMG is associated with an abundance profile (on the right) displaying the relative abundance of the contig across the 91 epi- and mesopelagic samples (based on normalized coverage, i.e. contig coverage / Gb of metagenome). **B.** Comparison of *sox*YZ-containing contigs maps. For contig GOV_bin_4310_contig-100_0, the second largest contig from the same bin (GOV_bin_4310_contig-100_1) is displayed. T4-like marker genes (Gp23 and T4 baseplate) are indicated on the maps, alongside putative AMGs (Fe-S biosyn: Iron-sulfur cluster biosynthesis).

Extended Data Figure 7: Diversity, distribution, and genome context of P-II genes in GOV contigs. A. Maximum-likelihood tree (from an amino-acid alignment) including the 10 viral P-II and microbial sequences from microbial metagenomes and NCBI nr database. The affiliation of microbial clades (either from the NCBI reference or from the LCA affiliation of metagenomic contigs) is indicated by coloring of the grouped clades or with a colored square next to the sequence. The sequences lacking the conserved uridylation site of P-II (Supplementary Fig. 5) are highlighted with a star next to the sequence name or clade. Viral AMG sequences are highlighted in blue, internal nodes SH-like supports are represented by proportional circles (all nodes with support < 0.40 were collapsed). Each P-II AMG is associated with an abundance profile (on the right) displaying the relative abundance

of the contig across the 91 epi- and mesopelagic samples (based on normalized coverage, i.e. contig coverage / Gb of metagenome). **B.** Comparison of P-II-containing contigs maps. Ammonia transporter genes linked to P-II are indicated on the map (Amm Transp, dark red). When available, the VC affiliation of each contig is indicated next to the contig name. Contig GOV_bin_5834_contig-100_7 is too short to be clustered based on a shared PC network, however the seed contig of its population was clustered (in VC_12, *Siphoviridae* - *P12024virus*), hence this seed contig affiliation is indicated.

Extended Data Figure 8: Diversity, distribution, and genome context of *amo*C gene in GOV contigs. A. Maximum-likelihood tree (from an amino-acid alignment) including the GOV *amo*C AMG and microbial sequences from microbial metagenomes and NCBI nr database. The affiliation of microbial clades (either from the NCBI reference or from the LCA affiliation of metagenomic contigs) is indicated by coloring of the grouped clades or with a colored square next to the sequence. Viral AMG sequence is highlighted in blue, internal nodes SH-like supports are represented by proportional circles (all nodes with support < 0.40 were collapsed). **B.** Abundance profile displaying the relative abundance of the contig across the 91 epi- and mesopelagic samples (based on normalized coverage, i.e. contig coverage / Gb of metagenome). **C.** Map of the *amo*C-containing contig.

Extended Data Figure 9: Normalized coverage of contigs harboring AMG as function of the temperature and nutrient concentrations (NO_2, NO_3, PO_4) of the corresponding samples. AMGs are grouped by clade based on the phylogeny (see Extended Data Fig. 5-6-7), and coverages are cumulated when a clade included multiple contigs. Plots display the cumulated normalized coverage of a clade (y-axis) as function of the temperature or nutrient concentration (x-axis) across all epipelagic samples (mesopelagic samples were excluded from the analysis since the AMG signal was detected in epipelagic samples), only for clades not geographically restricted (i.e. found in >5 samples, see Fig. 3C). Samples are color-coded according to their ocean and sea region (Supplementary Table 1). The calculated preferential range of temperature or nutrient concentration is displayed below each plot for the epipelagic AMGs (P-II-4 distribution could not be linked to specific environmental conditions, but this AMG is the only one consistently retrieved in mesopelagic samples).

Extended Data Table 1: Summary of genes and contigs characteristics for new viral DsrC, SoxYZ, and P-II AMGs. Each gene is linked to its contig, and when available, to the corresponding viral cluster and predicted host (from BLAST hit, CRISPR spacer similarity, or nucleotide composition similarity, Alphaprot.-Alphaproteobacteria, Gammaprot.-Gammaproteobacteria). Widespread and abundant VCs are highlighted in bold. In addition, the calculated pN/pS of each gene is indicated (measuring the strength of selection pressure occurring for this gene, the gene with a pN/pS not representing a strong purifying selection is highlighted in red), as well as the coverage of these genes and other genes in the contigs in 3 metatranscriptomic samples from 3 open ocean Tara stations (cases where the AMG coverage is >0.5 and associated with the coverage of other genes from the same viral contig are highlighted in green).

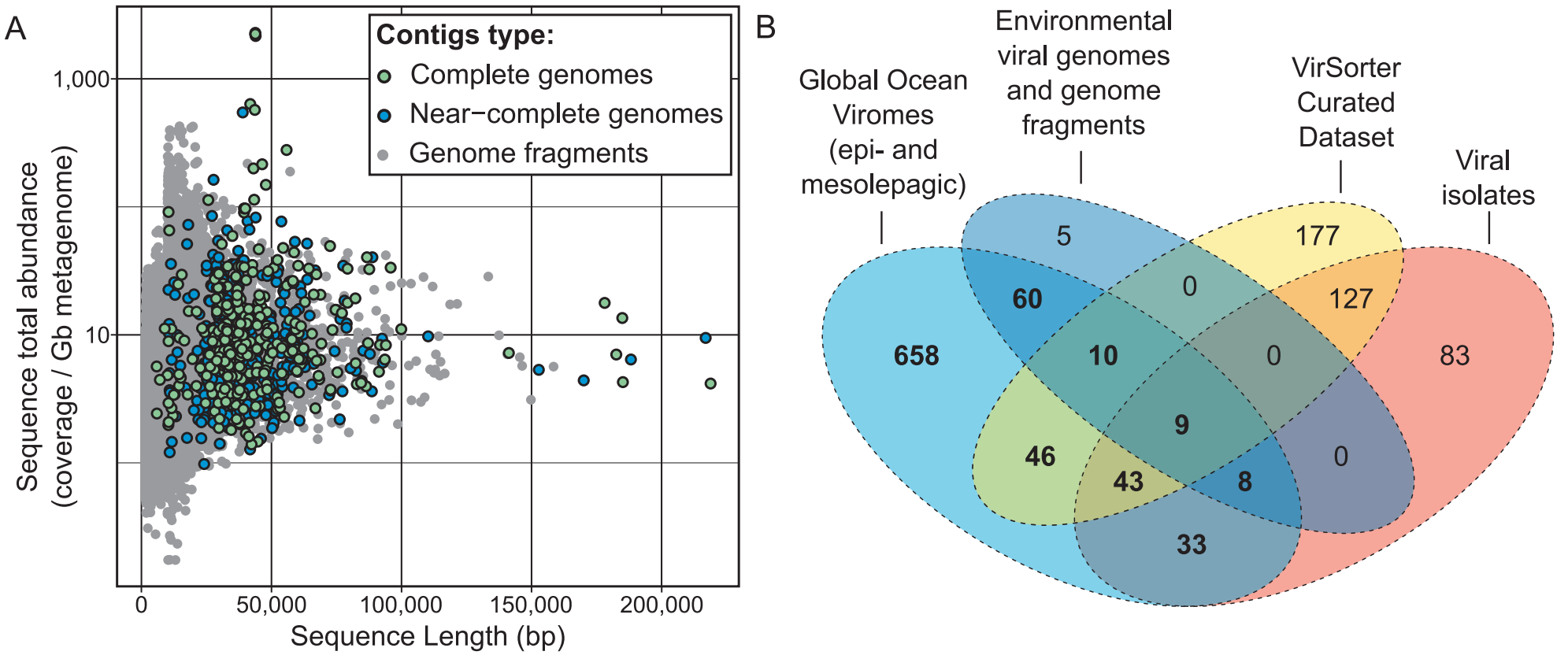
A
Contigs type:
Complete genomes
Near−complete genomes
Genome fragments
1,000
10
Sequence total abundance
(coverage / Gb metagenome)
0
50,000
100,000
150,000
200,000
Sequence Length (bp)
B
Global Ocean
Viromes
(epi- and
mesolepagic)
Environmental
viral genomes
and genome
fragments
VirSorter
Curated
Dataset
Viral
isolates
658
5
60
10
0
177
127
0
83
46
9
43
8
0
33

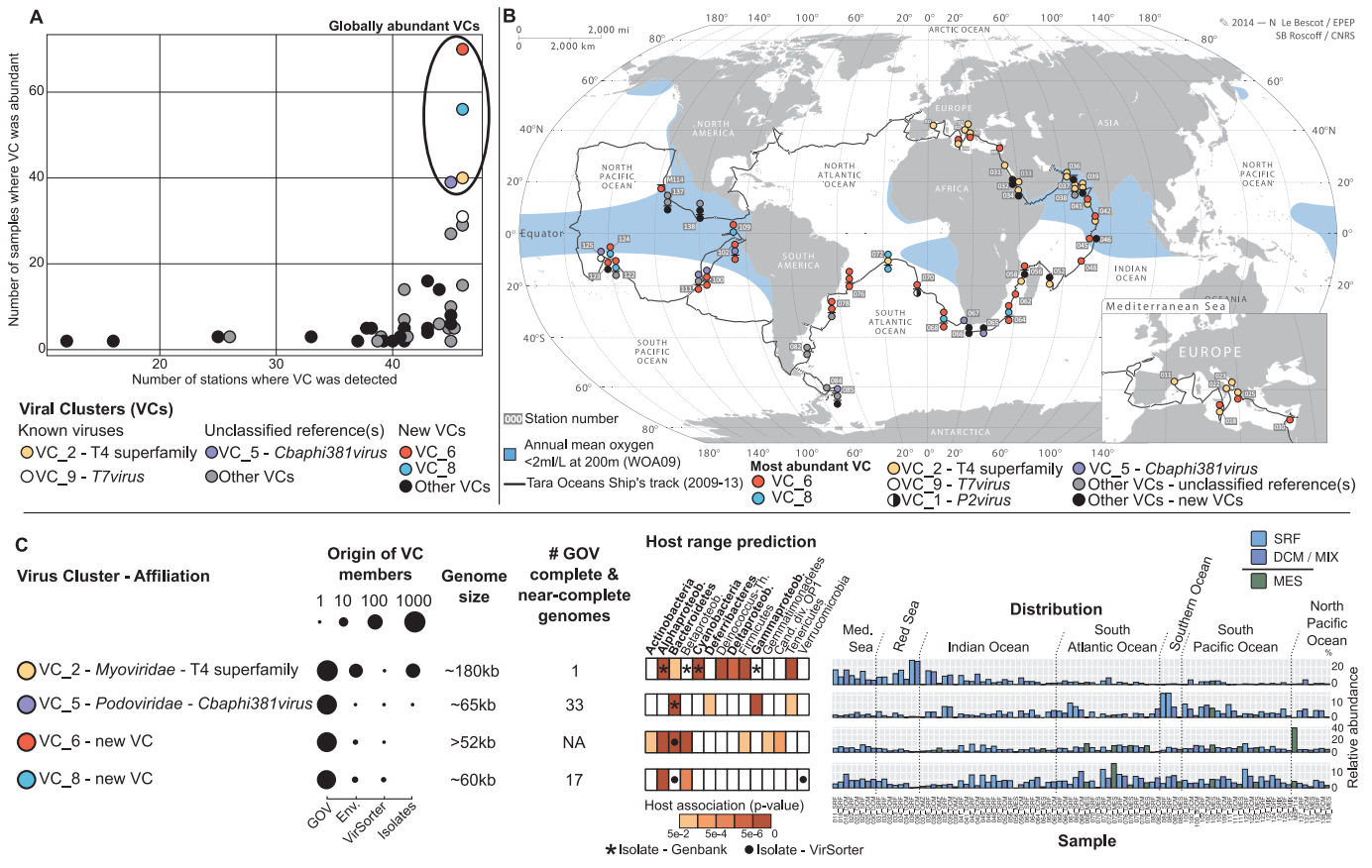
A
Globally abundant VCs
Number of samples where VC was abundant
Number of stations where VC was detected
Viral Clusters (VCs)
Known viruses
VC_2 - T4 superfamily
VC_9 - T7virus
Unclassified reference(s)
VC_5 - Cbaphi381virus
Other VCs
New VCs
VC_6
VC_8
Other VCs
B
2014 — N. Le Bescot / EPEP
SB Roscoff / CNRS
ARCTIC OCEAN
NORTH AMERICA
EUROPE
ASIA
NORTH PACIFIC OCEAN
NORTH ATLANTIC OCEAN
AFRICA
SOUTH AMERICA
INDIAN OCEAN
SOUTH ATLANTIC OCEAN
SOUTH PACIFIC OCEAN
OCEANIA
ANTARCTICA
Equator
Mediterranean Sea
Station number
Annual mean oxygen <2ml/L at 200m (WOA09)
Tara Oceans Ship's track (2009-13)
Most abundant VC
VC_6
VC_8
VC_2 - T4 superfamily
VC_9 - T7virus
VC_1 - P2virus
VC_5 - Cbaphi381virus
Other VCs - unclassified reference(s)
Other VCs - new VCs
C
Virus Cluster - Affiliation
Origin of VC members
1 10 100 1000
Genome size
GOV complete & near-complete genomes
VC_2 - Myoviridae - T4 superfamily
~180kb
1
VC_5 - Podoviridae - Cbaphi381virus
~65kb
33
VC_6 - new VC
>52kb
NA
VC_8 - new VC
~60kb
17
GOV
Env.
VirSorter
Isolates
Host range prediction
Actinobacteria
Bacteroidetes
Cyanobacteria
Deferribacteres
Fusobacteria
Gemmatimonadetes
Planctomycetes
Verrucomicrobia
Host association (p-value)
5e-2 5e-4 5e-6 0
Isolate - Genbank
Isolate - VirSorter
SRF
DCM / MIX
MES
Distribution
Med. Sea
Red Sea
Indian Ocean
South Atlantic Ocean
Southern Ocean
South Pacific Ocean
North Pacific Ocean
Relative abundance
Sample

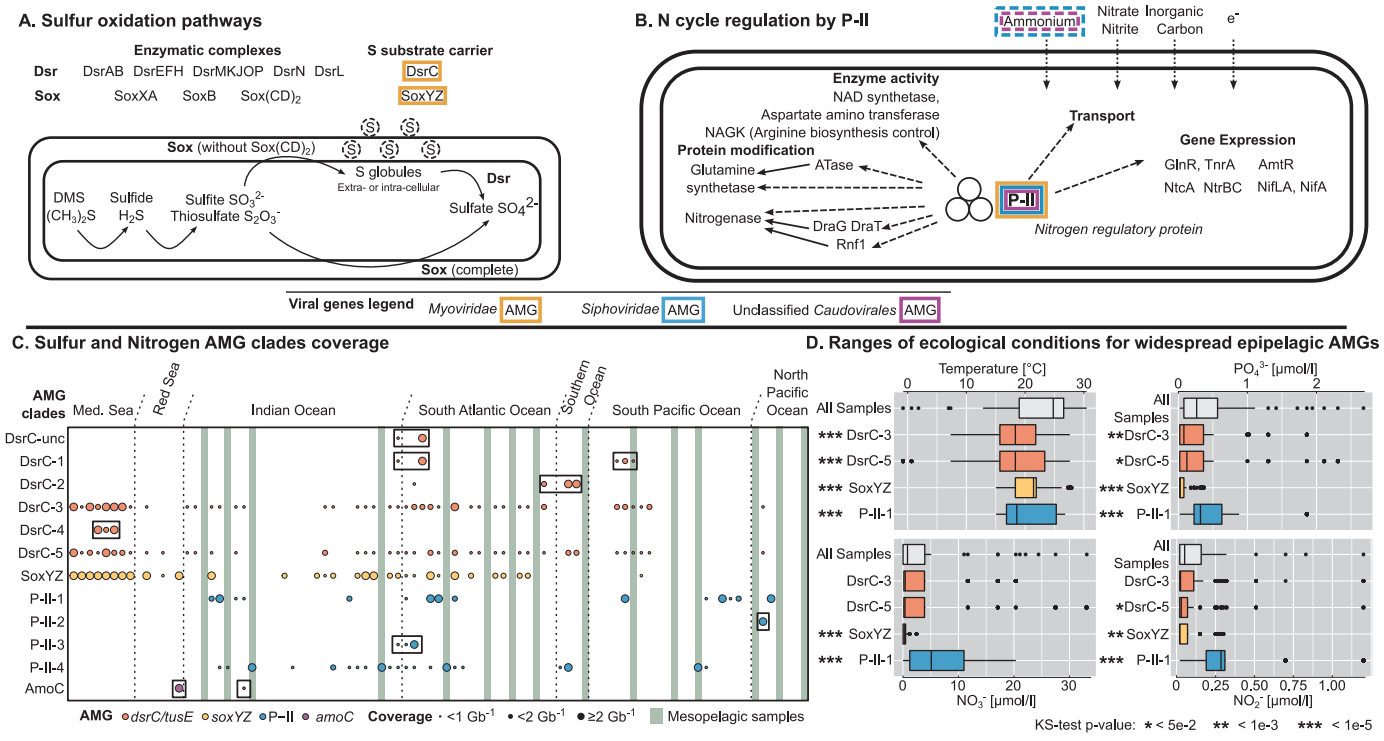
A. Sulfur oxidation pathways
Enzymatic complexes
S substrate carrier
Dsr
DsrAB DsrEFH DsrMKJOP DsrN DsrL
DsrC
Sox
SoxXA SoxB Sox(CD)2
SoxYZ
Sox (without Sox(CD)2)
S globules
Extra- or intra-cellular
Dsr
DMS (CH3)2S
Sulfide H2S
Sulfite SO3 2-
Thiosulfate S2O3 -
Sulfate SO4 2-
Sox (complete)
B. N cycle regulation by P-II
Ammonium
Nitrate Nitrite
Inorganic Carbon
e-
Enzyme activity
NAD synthetase,
Aspartate amino transferase
NAGK (Arginine biosynthesis control)
Protein modification
Glutamine synthetase
ATase
Nitrogenase
DraG DraT
Rnf1
Transport
P-II
Nitrogen regulatory protein
Gene Expression
GlnR, TnrA AmtR
NtcA NtrBC NifLA, NifA
Viral genes legend
Myoviridae AMG
Siphoviridae AMG
Unclassified Caudovirales AMG
C. Sulfur and Nitrogen AMG clades coverage
AMG clades
Med. Sea
Red Sea
Indian Ocean
South Atlantic Ocean
Southern Ocean
South Pacific Ocean
North Pacific Ocean
DsrC-unc
DsrC-1
DsrC-2
DsrC-3
DsrC-4
DsrC-5
SoxYZ
P-II-1
P-II-2
P-II-3
P-II-4
AmoC
AMG dsrC/tusE soxYZ P−II amoC
Coverage · <1 Gb-1 • <2 Gb-1 ● ≥2 Gb-1
Mesopelagic samples
D. Ranges of ecological conditions for widespread epipelagic AMGs
Temperature [°C]
PO4 3- [µmol/l]
NO3- [µmol/l]
NO2- [µmol/l]
All Samples
*** DsrC-3
*** DsrC-5
*** SoxYZ
*** P-II-1
** DsrC-3
* DsrC-5
** SoxYZ
KS-test p-value: * < 5e-2 ** < 1e-3 *** < 1e-5